Lab on a Chip

Microfluidic on-demand droplet generation, storage, retrieval, and merging for single-cell pairing

Journal:	*Lab on a Chip*
Manuscript ID	LC-ART-10-2018-001178.R1
Article Type:	Paper
Date Submitted by the Author:	19-Dec-2018
Complete List of Authors:	Babahosseini, Hesam; National Institutes of Health, National Cancer Institute Misteli, Tom; National Cancer Institute, NIH DeVoe, Don; University of Maryland, Mechanical Engineering

Microfluidic on-demand droplet generation, storage, retrieval, and merging for single-cell pairing

Hesam Babahosseini[1,2], Tom Misteli[1], Don L. DeVoe[2*]
[1]National Cancer Institute, National Institutes of Health, Bethesda, MD, 20892, USA
[2]Department of Mechanical Engineering, University of Maryland, College Park, MD, 20742 USA

Abstract

A multifunctional microfluidic platform combining on-demand aqueous-phase droplet generation, multi-droplet storage, and controlled merging of droplets selected from a storage library in a single integrated microfluidic device is described. A unique aspect of the technology is a microfluidic trap design comprising a droplet trap chamber and lateral bypass channels integrated with a microvalve that supports the capture and merger of multiple droplets over a wide range of individual droplet sizes. A storage unit comprising an array of microfluidic traps operates in a first-in first-out manner, allowing droplets stored within the library to be analyzed before sequentially delivering selected droplets to a downstream merging zone, while shunting other droplets to waste. Performance of the microfluidic trap is investigated for variations in bypass/chamber hydrodynamic resistance ratio, micro-chamber geometry, trapped droplet volume, and overall flow rate. The integrated microfluidic platform is then utilized to demonstrate the operational steps necessary for cell-based assays requiring the isolation of defined cell populations with single cell resolution, including encapsulation of individual cells within an aqueous-phase droplet carrier, screening or incubation of the immobilized cell-encapsulated droplets, and generation of controlled combinations of individual cells through the sequential droplet merging process. Beyond its utility for cell analysis, the presented platform represents a versatile approach to robust droplet generation, storage, and merging for use in a wide range of droplet-based microfluidics applications.

1. Introduction:

Droplet-based microfluidic technology offers unique capabilities for a broad range of applications in biochemical analysis, biomedical assays, and microscale biosynthesis.[1] Droplet-based microfluidic systems provide precise control and reliable manipulation of individual droplets in space and time using picoliter-scale aqueous droplets compartmentalized by a surrounding immiscible fluid. Each droplet can serve as a discrete reactor volume, allowing isolated biological or chemical reactions to be performed, or as a small volume sample container for sample manipulation or transport of biological particles. A number of approaches have been reported for the manipulation of microfluidic droplets for individual basic operations including droplet generation, trapping, storing, sorting, and coalescence of multiple droplets to support various biomedical or biochemical applications.[2–6] However, the combination of these functions into an integrated microfluidic platform is necessary to enable seamless control over all unit operations.

Precise generation of individual droplets with controlled volume is the first critical step for droplet-based microfluidics. Droplet generation can be implemented by either passive or active on-chip methods.[7–9] The most common strategies for passive droplet formation are by shearing a dispersed phase fluid into discrete volumes by an immiscible continuous phase fluid in a T-junction,[10–12] or by pinching off droplets within a symmetric flow-focusing configuration[13–15]. To facilitate on-demand droplet formation with control over both droplet size and formation rate, active droplet generation techniques offer an alternative approach which makes use of external actuation mechanisms such as electrowetting,[16,17] electro-emulsification,[18,19] or pneumatic membrane valving. In the latter case, droplet generation can be controlled by varying the size of a focusing orifice[20–22] or by mechanically gating the dispersed phase flow.[23–26]

Significantly, these active approaches can be used for individual droplet generation with precise control over both timing and volume.

Trapping of individual droplets for monitoring, detection, or incubation of reaction processes or encapsulated biological materials is another important function. Furthermore, the ability to store droplets in multiple trap chambers and selectively retrieve specific droplets on demand is needed for many applications in droplet-based microfluidics. As with droplet generation, both passive and active techniques have been reported for droplet trapping. Droplets can be passively confined in discrete chambers using either hydrodynamic trapping[27–30] or surface-energy anchors[31,32]. While straightforward to implement, one disadvantage of such passive approaches is that trapping is non-specific. Active droplet trapping techniques have also been reported, in which on-demand trapping and releasing of selected droplets is achieved by external actuation using electrodes,[33] laser,[34] or acoustic[35].

Beyond droplet generation and trapping, on-demand droplet merging is another important functional step, enabling droplets with different compositions or contents to be combined into a single droplet with precise spatial and temporal control. Droplet merging can be induced by changing microchannel geometry using an expansion zone,[36,37] tapered channel,[38] or trifurcating junction[39] to decelerate the droplets, allowing adjacent droplets to collide and merge after draining the lubrication layer between the droplets.[40,41] Transportation and synchronization of pairs of droplets concurrently in the merging zone is always challenging in each of these approaches. Alternately, the incorporation of constrictions or an array of pillars or other obstacles in the microchannel can facilitate entrapment and droplet contact to induce merging.[3,42–44] Targeted droplets can also be entrapped in a confined microwell or other anchor site and induced to merge.[45–48] However, each of these approaches presents limitations on the size and number of droplet that can be effectively merged. In addition, active merging approaches using electrocoalescence,[49–53] dielectrophoresis,[54,55] electrowetting,[56] thermo-capillary,[57,58] magnetic,[59] or acoustic wave[60] actuation have been widely explored, although these techniques can add unwanted complexity to the system due to the need for integration of an additional transduction mechanism.

In this work, we describe a multifunctional microfluidic platform capable of active droplet generation, capture, and storage, together with selective merging of targeted droplets within a multilayer polydimethylsiloxane (PDMS) chip developed using the simple soft lithography technique. The system employs a microvalve actuator to produce on-demand pico-liter volume droplets with adjustable droplet size within a T-junction droplet generator. To immobilize the individual droplets, a novel microfluidic trap mechanism consisting of a chamber with bypass channels and an integrated microvalve is presented. The array of active traps allows droplets to be sequentially stored in defined locations, with pneumatic microvalves used to modulate flow through the traps, enabling the storage mechanism to control and immobilize individual droplets across a broad range of sizes. The array operates in a first-in, first-out (FIFO) manner. After filling the trap array, selected droplets are mobilized to the merging chamber, where controlled droplet fusion is induced. The same trap topology is also applied to achieve droplet merging within the system.

Here we explore the platform for application to the isolation of individual cells selected from different populations. Cell-cell communication and cell signaling is central to the regulation of many biological functions, such as cell proliferation, viability, motility, and differentiation.[61,62] The developed droplet-based microfluidic system provides an effective approach to generating, capturing, and storing droplets, followed by merging of the droplets containing individual cells of different types within a single droplet. This functionality may provide a new approach for studying cell signaling at the single cell level, offering potential for a wide range of studies involving cell-cell communication and paracrine signaling, such as cell signaling in tumor environments,[63] tumor/stem cell communications,[64] immune/non-immune cell communications, [65–67] bacterial quorum sensing,[68,69] and studies of cell signaling under the influence of exogenous factors.[70]

2. Materials and methods:

2.2 Microfluidic chip fabrication:

The microfluidic devices were manufactured by multi-layer soft-lithography using PDMS (Sylgard 184, Dow Corning, USA). Each device is composed of a top fluidic layer and a bottom pneumatic control layer bonded on a glass slide. The layers form three functional elements including the droplet generator, storage, and merging unit. A schematic diagram of the integrated microchip is shown in Fig. 1A. The fabrication process flow, which is based on a previously-demonstrated approach,[71] is shown in Fig. 1B. Briefly, master molds were obtained by spin-coating negative photoresist (SU-8 2075, Microchem Corp, Newton, MA) at 3500 rpm for 60 s to construct 40 μm thick structures on a silicon wafer. To form a 3 mm thick fluidic layer, the PDMS prepolymer and the curing agent mixture at 10:1 ratio was molded on the master mold, partially cured at 80 °C for 30 min and peeled off from the master mold. Access ports were formed in the fluidic layer using a punch. A 36 μm control layer was formed on the master mold by spin-coating the PDMS prepolymer and the curing agent mixture at a ratio of 20:1 at 1500 rpm for 1 min and partial curing at 80 °C for 10 min. The fluidic layer was then aligned on the control layer and fully cured at 80 °C overnight. The two-layer PDMS device was peeled off from the master mold, punched to introduce ports into the control layer, and then bonded to a glass slide using oxygen plasma treatment for 60 s. To enhance hydrophobicity following the plasma treatment, the chips were stored at 115 °C in an oven overnight.[72]

2.2. Device operation:

The microfluidic valves used for droplet formation, capture, release, and merging were operated by a solenoid valve manifold (Clippard Instrument Lab Inc., Cincinnati, OH) and an Arduino microcontroller board to provide individual switching of each 3-way solenoid valve. A custom code was developed to actuate the individual elastomer membrane microvalves. The solenoid valves were interfaced with the chip through urethane tubing (1.52 mm ID, 3.30 mm OD, Clippard) and 22 gauge needle segments (Hamilton, Reno, NV) inserted into the on-chip pneumatic access holes. Nitrogen gas was supplied to the solenoid valve manifold through a regulator (5–50 psi range, McMaster-Carr, Elmhurst, IL) at a pressure of 20 psi to control the microvalves.

For introducing liquids into the fluidic layer, each fluid was stored in a custom plastic container[73] and driven through the microfluidic by application of a constant pressure. For device characterization, the continuous oil phase consisted of light mineral oil with Span-80 surfactant at a 0.01% concentration (Sigma-Aldrich, St. Louis, MO), and the dispersed aqueous phase consisted of deionized (DI) water with dissolved blue or green food dyes. Nitrogen gas was applied to each oil-phase and aqueous-phase container using an independent regulator (0-10 psi range, Marsh Bellofram Co., Newell, WV). The liquids were introduced into the chip using flexible Tygon microbore tubing (0.51 mm ID, 1.52 mm OD, Cole-Parmer, Vernon Hills, IL) connected to 22 gauge needle segments inserted in the fluidic access holes.

The microfluidic chip was mounted onto an inverted microscope (Nikon AZ100), and images were captured with a high-resolution camera. Fluorescently labeled cells were monitored using an inverted fluorescence microscope (Nikon TE2000) equipped with a high sensitivity camera. The entire procedure for device operation including droplet generation, trapping, fluorescence monitoring of the droplet array, shunting of undesired droplets to waste, and merging of desired droplets can be accomplished within several minutes.

2.3. Cell sample preparation:

Human skin fibroblasts were grown in DMEM medium with 10% Fetal Bovine Serum (FBS), 2 mM glutamine, and penicillin/streptomycin and split 1:4 twice weekly. Cells were fixed in 4% paraformaldehyde for 20 min, washed and stored in phosphate-buffered saline (PBS) buffer. Cells were stained with either PicoGreen or DAPI dye and resuspended in PBS buffer, with the cell concentration adjusted based on Poisson statistics.[74,75]

3. Results and discussion:

3.1. Device design

As shown in Fig. 1, the microfluidic chip consists of three functional units, namely an on-demand droplet generation unit, a trapping and storage unit, and a droplet merging unit. In the droplet generation unit, a T-junction structure integrated with a pneumatic microvalve is used to produce discrete aqueous-phase droplets on demand, with control over both timing and droplet volume. The waste outlet 1 depicted in Fig. 1 is included in the design to allow fluids to be shunted out of the system ahead of the FIFO traps, as may be desired to clear residual fluid from the droplet generator channels before introducing new sample solutions into the chip. The generated droplets are then carried by the continuous oil phase into the FIFO storage unit composed of a linear array of microfluidic traps. In the storage unit, the droplets are sequentially captured in the traps to form a library of immobilized droplets. The first droplet traverses the full array to be stored in the most distal trap, while the last droplet is stored in the first trap proximal to the droplet generator. Stored droplets may be incubated and optically monitored. After screening, the droplets are released sequentially in a controlled manner, beginning with the first droplet entered the trap array. The released droplets move downstream, with selected droplets delivered to the merging unit, while undesired droplets are shunted to the waste outlet 2. In the merging unit, the incoming droplets coalesce and fuse together to produce a combined droplet with desired volume and composition. In the device design explored here, the width of the main flow channel is 60 μm, while other fluidic channels and pneumatic control channels are 100 μm wide.

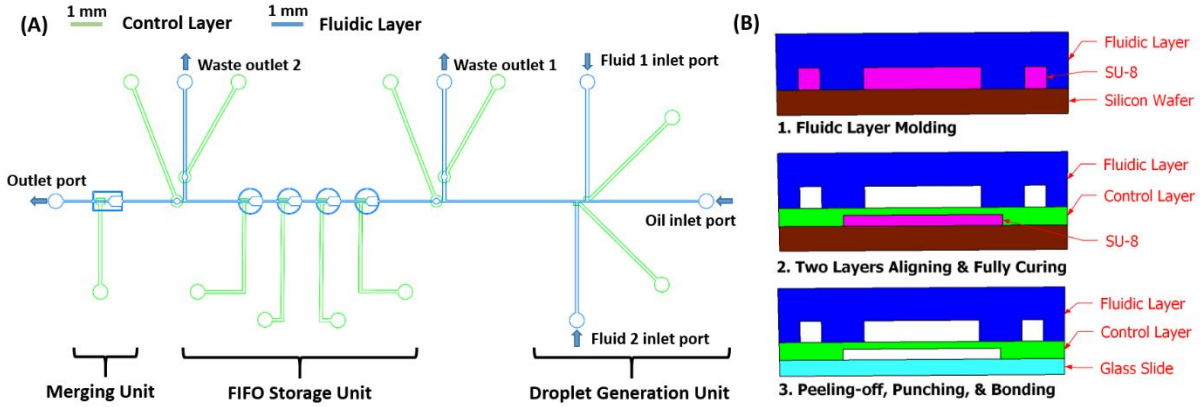

Figure 1. Design and layout view of the integrated microfluidic chip including droplet generators, FIFO storage with an array of microfluidic traps, and merging mechanism. B) Process flow for fabrication of the microchip.

3.2. On-demand droplet generation

The aqueous phase droplets are generated on demand using a previously reported design,[23–26] in which an elastomer microvalve is used to modulate the flow and discretization of an aqueous phase within a continuous oil phase at a T-junction. In the present design (Fig. 2), two perpendicular channels facing each other are used for the dynamic droplet generation process. A microvalve is used at each T-junction to physically block the flow of the aqueous phase and trigger droplet formation. Using this approach, droplets with defined volume are generated on demand by opening the microvalve for a specified period using programmed actuation (Video S1).

The effects of inlet pressure and valve period on droplet size were studied, with the results shown in Fig. 2B. For a given dispensing time, droplet volume was found to increase with a higher inlet pressure ratio between the aqueous (P_{aq}) and oil (P_{oil}) phases. This result reflects the fact that the fluid volume ejected from the aqueous flow channel scales with the pressure difference between the aqueous inlet and

intersection with the continuous phase channel, which itself depends on both the oil inlet pressure and total flow rate within the system. Similarly, when holding the inlet pressures at a fixed ratio, the droplet size was observed to scale proportionally with the dispensing time. Using this approach, controllable volumes ranging from approximately 100-800 pL were achieved for the fabricated droplet generators. Each droplet generation microvalve employs a 36 μm thick elastomer membrane with a 100 μm × 100 μm footprint over a 40 μm deep T-junction. The dimensions were selected based on previous reports for reliable push-up microvalve[76] and T-junction[77] geometries. For this design, uniform formation of droplet volumes as low as 100 pL, corresponding to an open valve period of 400 ms, were reliably achieved. Smaller droplet volumes were found to be irreproducible, presumably due to the limited mechanical response of the microvalves. With dispensing times above the range shown for each condition in Fig. 2B, the generation of multiple droplets was often observed due to shear-induced discretization of the dispersed phase before closing the microvalve.

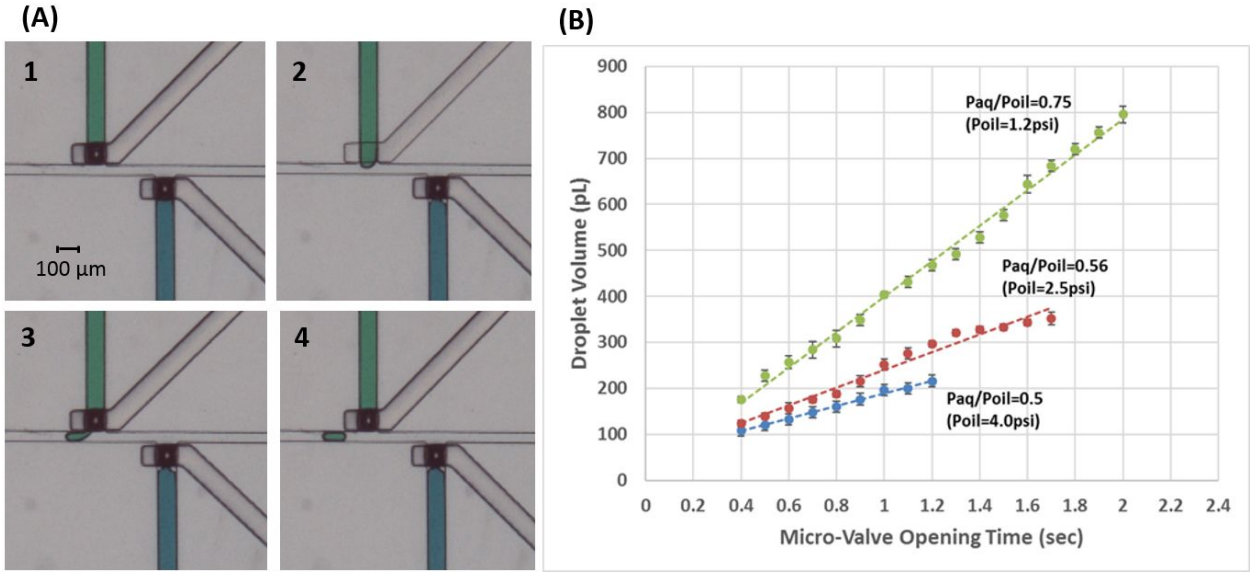

Figure 2. A) Sequential images showing the on-demand droplet generation process. B) Effects of valve opening time and ratio of inlet pressures for the aqueous and oil phases (P_{aq}/P_{oil}) on droplet volume. Error bars represent standard deviations for multiple measurements (n=3) in a single device.

3.3. Droplet capture and release

A microfluidic trap mechanism was developed for passive capture and controlled release of individual droplets. Each microfluidic trap comprises a chamber for trapping and storing droplets, two parallel bypass flow paths, and a downstream channel with an integrated microvalve that serves to modulate hydraulic resistance to flow through the chamber. The detailed geometry of a microfluidic trap is shown in Fig. 3A, and a hydraulic resistance circuit diagram of the trap is shown in Fig. 3B. In this design, the integrated microvalve serves to control the relative flow rates through the chamber and bypass channels. When the valve is open, droplets traverse the trap volume and exit the chamber through the downstream channel. To selectively capture droplets within the chamber, the valve is actuated, increasing the hydrodynamic resistance of the trap flow path without fully occluding the flow. When the valve is actuated, droplets enter the chamber, where the circulating streamlines deliver the droplets to a stagnation zone, typically located at the point where the chamber begins to taper toward the downstream exit channel, thereby trapping them within the chamber. In this configuration, the majority of the continuous phase flow is shunted through the parallel bypass channels. For controlled release, the microvalve is turned off, allowing the incoming continuous phase to flow primarily through chamber and eject the trapped droplet through the downstream

channel. Simulations of this process generated using COMSOL software are shown in Fig. 3C and 3D, revealing the continuous phase flow streamline distributions for microvalve on and off states, respectively.

The hydraulic resistance ratio between the main trap flow path (R_{trap}) and parallel bypass channels (R_{bypass}) is an important parameter that impacts the performance of the droplet capture and release processes. Under laminar flow conditions, the hydraulic resistance of a channel with rectangular cross-section can be approximated as:

$$R = 2\mu L(P^2/A^3) \tag{1}$$

where μ is the fluid viscosity, L is the channel length, and P and A are the perimeter and area of the channel cross-section, respectively. Applying the given trap geometry to Eq. 1, the following expression is obtained:

$$\frac{R_{trap}}{R_{bypass}} = \frac{\dfrac{2\mu L_c(2W_c+2H)^2}{W_c^3H^3} + \int_{W_n}^{W_c}\dfrac{2\mu L_g(2W+2H)^2}{W^3H^3} + \dfrac{2\mu L_n(2W_n+2H)^2}{W_n^3H^3}}{2.\dfrac{2\mu L_b(2W_b+2H)^2}{W_b^3H^3}} \tag{2}$$

$$\frac{R_{trap}}{R_{bypass}} = \frac{L_cW_b^3(W_c+H)^2}{2L_bW_c^3(W_b+H)^2} + \frac{L_gW_b^3}{4L_b(W_b+H)^2(W_c-W_n)}\left(Ln\left(\frac{W_c}{W_n}\right)+\frac{H^2}{2}\left(\frac{1}{W_n^2}-\frac{1}{W_c^2}\right)+2H\left(\frac{1}{W_n}-\frac{1}{W_c}\right)\right)+\frac{L_nW_b^3(W_n+H)^2}{2L_bW_n^3(W_b+H)^2} \tag{3}$$

where the variables of bypass channel, chamber, gradual contraction section, and narrow path are represented by subscript b, c, g, and n, respectively.

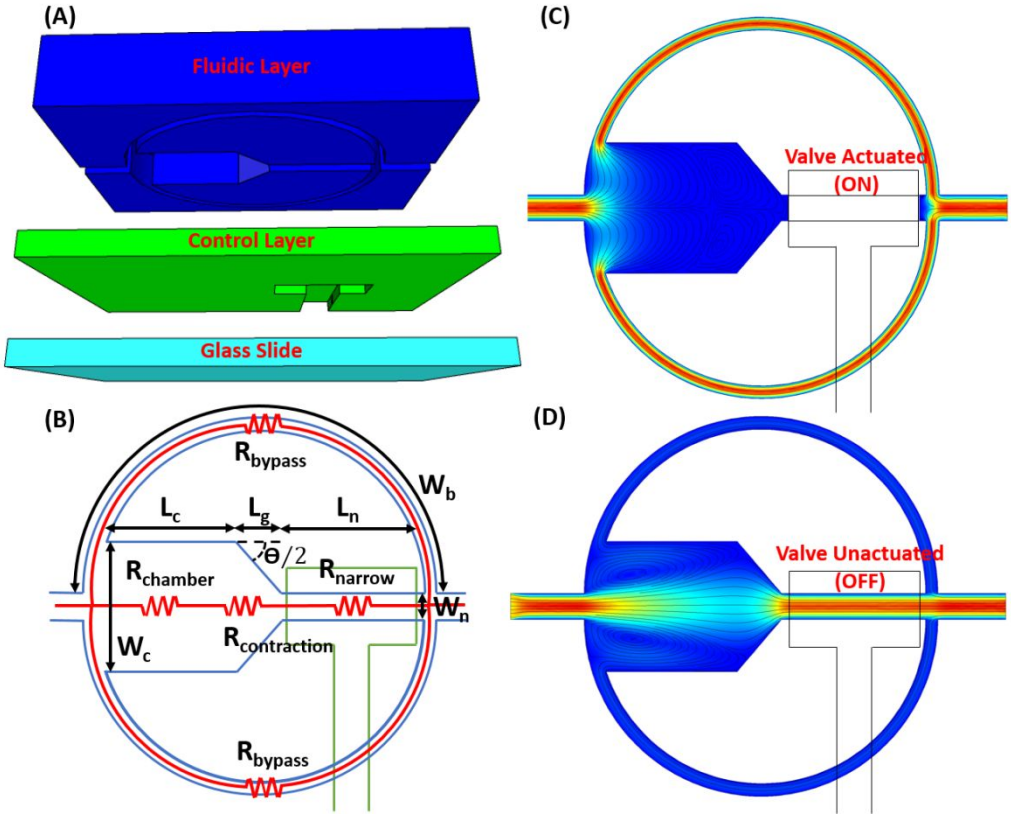

Figure 3. Detailed design and working principle of the microfluidic trap mechanism; A) 3D exploded illustration of a microfluidic trap. B) Circuit diagram summarizing the various contributions to hydraulic resistance across the trap.

Numerical simulations of the microfluidic trap with the microvalve in its C) actuated (ON) and D) unactuated (OFF) states.

A set of experiments were conducted to evaluate the operational domains of the microfluidic trap by changing the droplet diameters and the effective parameters in the trap design including the hydraulic resistance ratio (R_{trap}/R_{bypass}) and the chamber taper angle (Θ; see Fig. 3B). Experiments were performed with the diameter of the droplet produced by the upstream on-demand generators ranging from 40 to 130 μm and chamber taper angle ranging from 120° to 155°. To vary the hydraulic resistance ratio (R_{trap}/R_{bypass}), the bypass width was varied between 20 and 35 μm, resulting in the ratios varying between 1.7 and 6.0 percent as determined by Eq. 2 for the given trap dimensions (W_c = 300 μm, W_n = 60 μm, L_b = 1005 μm, L_c = 300 μm, L_g = 100 μm, L_n = 300 μm, and H = 40 μm). In addition, experiments were performed under two different continuous phase flow rates of 1.2 nL/s and 2.4 nL/s, with the results of these experiments presented in Fig. 4 and Fig. 5, respectively. As revealed in these figures, three distinct operational domains were observed with domain boundaries dependent on system parameters including hydraulic resistance ratio, droplet size, and bulk flow rate. In the first domain, droplets are successfully captured within the chamber when the exit valve is closed, and successfully released from the chamber upon valve opening. In this regime, droplet capture occurs at stagnation zones located at the obtuse-angled chamber corners, with capture more readily achieved when operating at a total bulk flow rate of 1.2 nL/s (Fig. 4) compared to 2.4 nL/s (Fig. 5) where higher flow-induced stresses act on the droplets during trapping. In the second regime, droplets cannot be captured in the chamber, and are instead shunted through the closed chamber exit valve, which cannot be fully sealed due to the rectangular cross-sectional geometry of the channel beneath the elastomer film. This shunting behavior is observed as droplet size increases and the droplet is exposed to streamlines that prevent it from entering the stagnation zone. Similarly, as the hydraulic resistance ratio decreases due to a reduction in bypass channel width, the stagnation zone volume is reduced, preventing capture of smaller droplets. In the third regime, droplets are successfully captured, but cannot be expelled from the trap for a given continuous phase flow rate, resulting in unsuccessful release. This regime occurs for smaller droplets and larger hydraulic resistance ratios, where the flow rate through the open trap is insufficient to displace droplets from the stagnation zone. The boundaries between the three domains is also dependent on chamber taper angle. As taper angle increases, larger average flow velocity is imposed within the corner region, reducing the droplet size and increasing the hydraulic resistance ratio for which successful capture can occur.

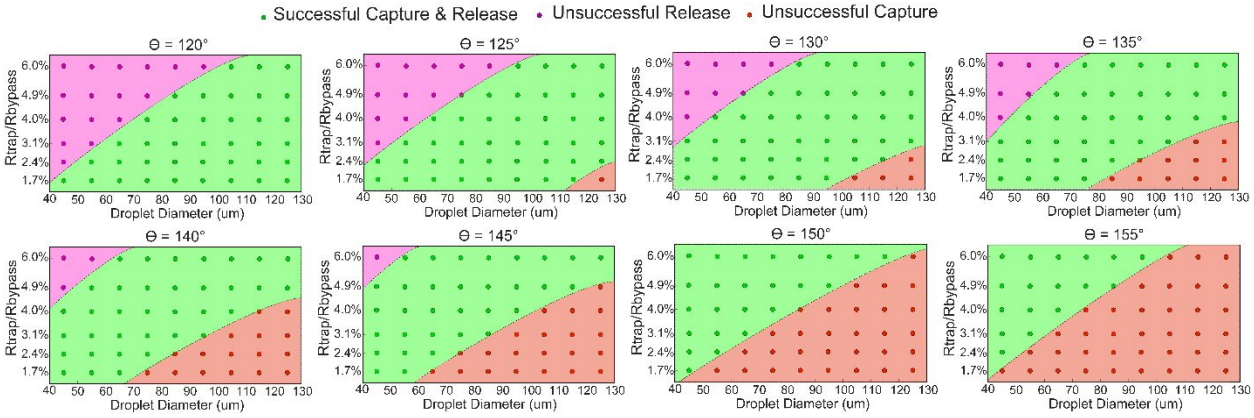

Figure 4. Effect of droplet size, hydraulic resistance ratio (R_{trap}/R_{bypass}), and trap chamber taper angle on droplet capture and release when imposing a volumetric flow rate of 1.2 nL/s.

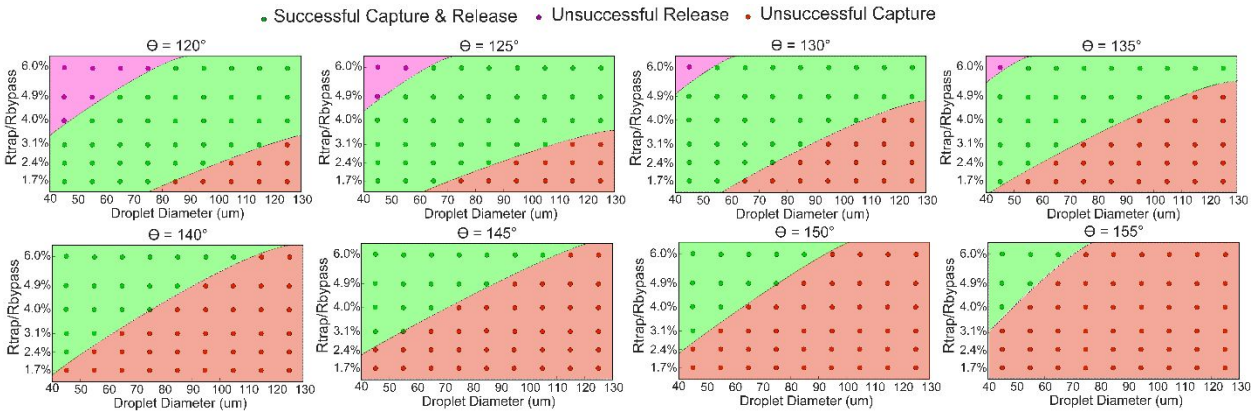

Figure 5. Effect of droplet size, hydraulic resistance ratio (R_{trap}/R_{bypass}), and trap chamber taper angle on droplet capture and release when imposing a volumetric flow rate of 2.4 nL/s.

3.4. Sequential FIFO loading and unloading

Droplets formed by the droplet generation units are transported into the trap array by convective flow. As the first droplet enters the array, the valve associated with the last trap is actuated, thereby capturing the droplet within this trap. This sequence is repeated for each additional trap, until single droplets have been sequestered within all of traps in the array. Based on this simple principle, the storage unit can be loaded to form a static droplet library (Fig. 6A). In the trap design, the microvalve channel passes over one of the bypass channels, and thus when the valve is actuated the resulting deflection of the membrane over the bypass channel may increase the hydrodynamic resistance within that branch. However, membrane deflection nominally scales with the 4th power of membrane width,[78] and the resulting deflection has been calculated to be less than 1 um over a 100 µm channel length, resulting in a negligible impact on flow distribution. A unique advantage of this storage unit is its capability to produce a droplet network with varying droplet size or composition. Fig. 6 shows sequential images of loading and unloading a FIFO storage array with four droplets (Video S2 and S3). The droplets are formed with ascending diameters of approximately 70, 80, 100, and 110 µm to demonstrate the capability of the platform to controllably generate and capture droplets with varying size. After optically monitoring the stored droplets to identify selected droplets for merging, the storage unit can be unloaded by sequentially releasing the trapped droplets, starting with the last trap that was used to immobilize the first droplet introduced into the array (Fig. 6B). After releasing the droplets, a downstream flow splitter with an integrated elastomer microvalve serves to guide each droplet either to waste or to the merging unit (Video S4).

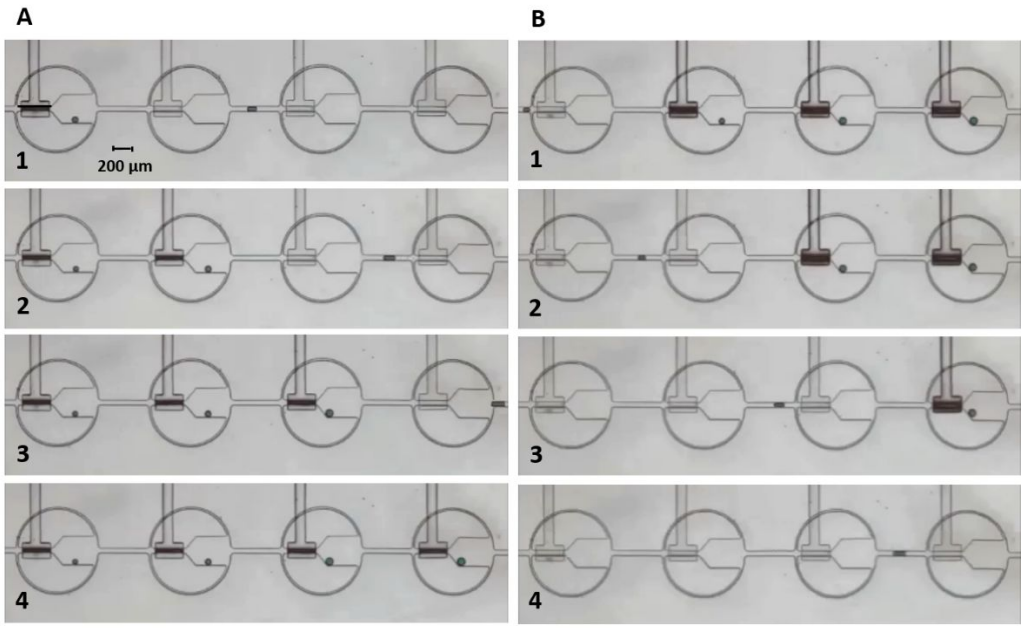

Figure 6. FIFO storage operation: sequential images of (A) droplet loading in the FIFO storage array for screening and (B) droplet unloading from the array. Released droplets are selectively guided to the merging unit or shunted to waste.

3.5. Droplet merging:

The droplets selected from the storage library are transported to the merging unit. The merging element is topologically identical to the traps used for droplet capture and release, but with a chamber volume designed to accommodate multiple droplets. In the merging process, the downstream chamber valve is closed as multiple droplets are driven sequentially into the merging chamber. Within the chamber, incoming droplets coalesce and fuse with the previously stored droplet as the oil film between two droplets is drained out. A recorded merging sequence of multiple droplets is shown in Fig. 7. Passive merging of the selected droplets occurs rapidly, with typical merging times below 1 s observed after collision in the trap zone (Video S4).

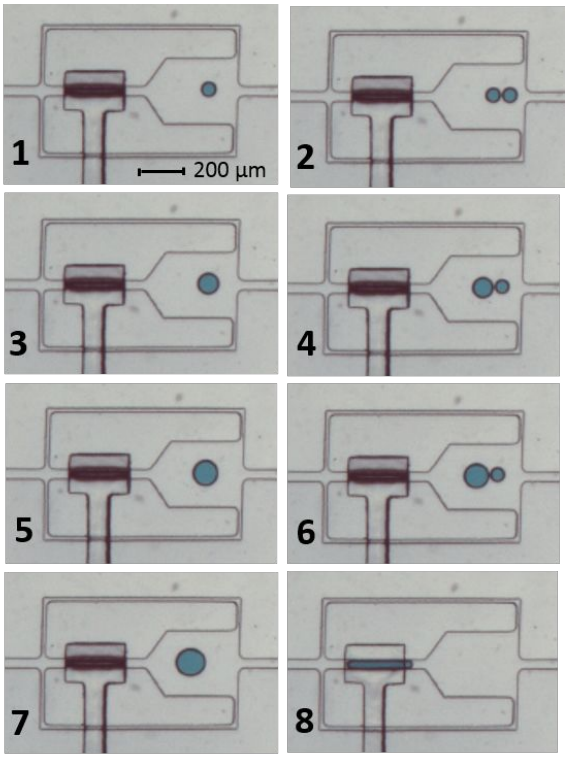

Figure 7. Droplet merging process. Two droplets are sequentially introduced into the merging chamber, followed by passive coalescence over a period of approximately 0.24 s. After merging, the chamber valve is opened, releasing the combined droplet from the merging zone.

3.6. Single cells encapsulation, screening, and pairing:

To demonstrate the capabilities of the multifunctional platform, an experiment was conducted with biological cells to document the full set of functional steps including individual droplet generation, trapping, storing, releasing, and selective merging. The goal is to form final merged droplets containing a pre-determined number of cells (from 2 to 6) and ratio of two cell types (from 1:1 to 3:3 for each type).

Two individual solutions of mammalian cells either stained with blue (DAPI) or green (PicoGreen) DNA dyes were connected to the inlets of the two droplet generators, allowing cell-encapsulating droplets to be generated on-demand. For each cell solution, droplets were sequentially formed and the FIFO storage unit is loaded with the individual droplets containing each cell type. The droplets were screened in the storage taps by fluorescence microscopy, and two droplets containing the desired number of each cell type were then guided to the merging unit for a final merging. Using this approach, a single droplet isolating a controlled mixture of both cell types was obtained. Fig. 8 shows a matrix of merged droplets with a pre-determined number and ratio of the two cell types. This demonstration reveals the capability of the chip for the generation of specified cell populations with control at the single cell level.

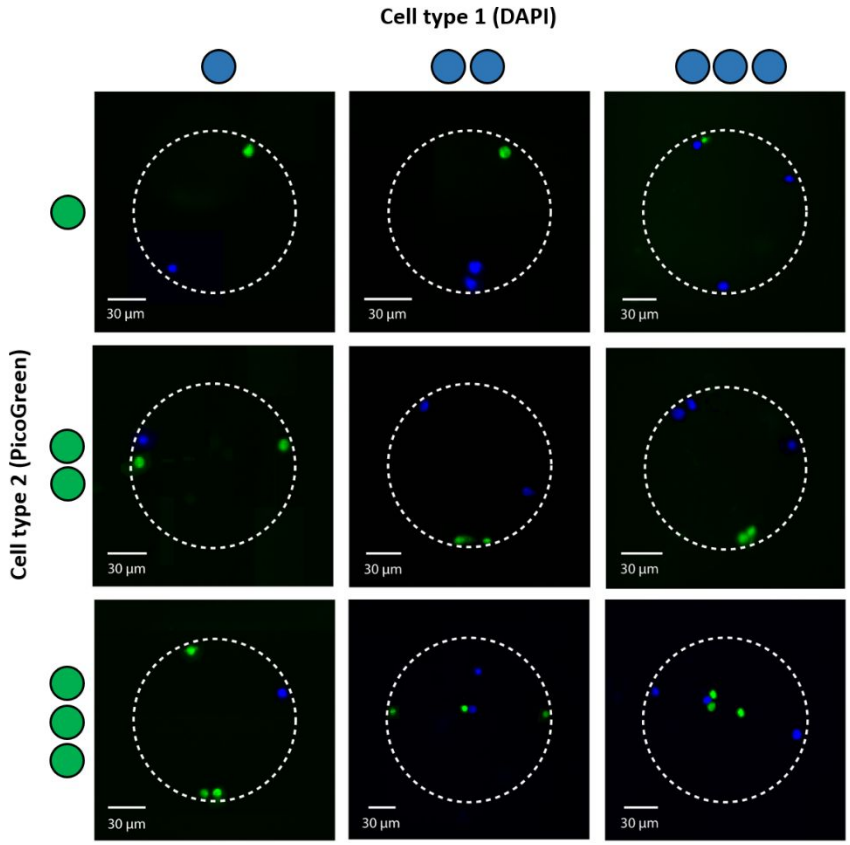

Figure 8. Controlled formation of defined cell populations by droplet generation and selective merging in the microfluidic system. The final merged droplets contain a pre-determined number of cells (from 2 to 6) and ratio of cell types (from 1:1 to 3:3 for each type).

Discussion:

Due to the discrete nature of the cell encapsulation process, the number of cells present in each aqueous volume formed by the droplet generation unit follows a Poisson distribution.[73,74] the For cell concentration (2×10^6 cells/mL) and typical droplet volume (approximately 250 pL) used in this work, the probabilities for a single droplet to encapsulate a given number of cells are approximately 27% for 1 cell, 27% for 2 cells, and 18% for 3 cells. In our experiments (n=36), the measured distribution probabilities for each case were 25.0%, 30.5%, and 19.4%, respectively. While each trap loading experiment performed here resulted in at least one captured droplet each with 1 cell and 2 cells, generation of a droplet with 3 cells was not always observed due to the lower probability of this event and the limited number of trap chambers.

A total of 7 microvalves were employed to control all unit operations including 2 droplet generators, 4 droplet storage mechanisms, and 1 merging unit, with an additional 4 microvalves used to control flow to the waste outlets. The microvalve states are readily defined using an Arduino microcontroller and off-chip solenoid valve board for pneumatic control, allowing the entire procedure for droplet generation, storage, and merging to be accomplished in a programmable and synchronized fashion. Specifically, two droplet generators are first actuated to form on-demand droplets in an automatic process. After each droplet formation event, the resulting droplet travels in the main channel to reach to the last trap mechanism in the array of trap mechanisms where the microvalve must be closed for capturing the droplet. The traveling time of each droplet carried by the continuous-phase oil with a constant flow rate to reach to a specific trap mechanism can be calculated (for instance, it takes approximately 12.0 sec for a 300 pL droplet to travel to the last trap mechanism via a 1.2 nL/s continuous-phase oil flow rate). After loading the storage unit, the

stored droplets could be monitored automated by the image-processing technique and the desired droplets with adequate number of cells are selected for transferring into the merging mechanism. Same as before, with a good estimation, the total time required for a droplet to reach either the waste line or the merging mechanism is measured. As a result, the entire procedure for generation and handling the droplets can be accomplished in a fast fashion within a few minutes.

Although the cells are not expected to come into contact spontaneously after droplet merging, the droplets put the cells in close vicinity, offering potential for a wide range of cell-cell communication studies involving contact-independent secretory mechanisms such as paracrine signaling.[65,66]

Conclusion:

The described device allows for the execution of multiple steps of on-demand droplet generation, individual storage of droplets in addressable chambers, consecutive retrieval of stored droplets, and controlled merging of a selected droplets sequence containing desired reagents or cells. Here, the microfluidic platform was employed to enable the precise entrapment, isolation, monitoring, and pairing of different combinations of individual cells within discrete droplets. The integrated droplet-based microfluidic device provides a robust hardware platform with potential for a wide range of applications requiring controlled droplet manipulation, and particular benefits for fundamental studies in the field of cell-cell communication and paracrine signaling.

Supplementary Information:

Movie S1. Droplet generation on-demand

Movie S3. Droplet loading in the FIFO storage

Movie S4. Droplet unloading from the FIFO storage

Movie S4. Multiple droplet merging process

References:

1 L. Shang, Y. Cheng and Y. Zhao, *Chem. Rev.*, 2017, **117**, 7964–8040.
2 S. H. Jin, H.-H. Jeong, B. Lee, S. S. Lee and C.-S. Lee, *Lab Chip*, 2015, **15**, 3677–3686.
3 X. Chen, A. Brukson and C. L. Ren, *Microfluid. Nanofluidics*, 2017, **21**, 1–10.
4 R. Seemann, M. Brinkmann, T. Pfohl and S. Herminghaus, *Reports Prog. Phys.*, 2012, **75**, 016601 (41pp).
5 S.-Y. Teh, R. Lin, L.-H. Hung and A. P. Lee, *Lab Chip*, 2008, **8**, 198.
6 H.-H. Jeong, B. Lee, S. H. Jin, S.-G. Jeong and C.-S. Lee, *Lab Chip*, 2016, **16**, 1698–1707.
7 P. Zhu and L. Wang, *Lab Chip*, 2017, **17**, 34–75.
8 A. Huebner, S. Sharma, M. Srisa-Art, F. Hollfelder, J. B. Edel and A. J. deMello, *Lab Chip*, 2008, **8**, 1244.
9 H. Gu, M. H. G. Duits and F. Mugele, *Int. J. Mol. Sci.*, 2011, **12**, 2572–2597.
10 T. Thorsen, R. W. Roberts, F. H. Arnold and S. R. Quake, *Phys. Rev. Lett.*, 2001, **86**, 4163–4166.
11 A. Gupta, S. M. S. Murshed and R. Kumar, *Appl. Phys. Lett.*, 2009, **94**, 16–18.
12 P. Garstecki, M. J. Fuerstman, H. A. Stone and G. M. Whitesides, *Lab Chip*, 2006, **6**, 437.
13 R. Dreyfus, P. Tabeling and H. Willaime, *Phys. Rev. Lett.*, 2003, **90**, 4.
14 S. L. Anna, N. Bontoux and H. A. Stone, *Appl. Phys. Lett.*, 2003, **82**, 364–366.
15 L. Yobas, S. Martens, W.-L. Ong and N. Ranganathan, *Lab Chip*, 2006, **6**, 1073.

16 H. Gu, M. H. G. Duits and F. Mugele, *Lab Chip*, 2010, **10**, 1550.
17 H. Gu, F. Malloggi, S. A. Vanapalli and F. Mugele, *Appl. Phys. Lett.*, 2008, **93**, 1–4.
18 H. Kim, D. Luo, D. Link, D. A. Weitz, M. Marquez and Z. Cheng, *Appl. Phys. Lett.*, 2007, **91**, 1–4.
19 P. He, H. Kim, D. Luo, M. Marquez and Z. Cheng, *Appl. Phys. Lett.*, 2010, **96**, 2008–2011.
20 A. R. Abate, M. B. Romanowsky, J. J. Agresti and D. A. Weitz, *Appl. Phys. Lett.*, 2009, **94**, 1–4.
21 C. Y. Lee, Y. H. Lin and G. Bin Lee, *Microfluid. Nanofluidics*, 2009, **6**, 599–610.
22 S. K. Hsiung, C. T. Chen and G. Bin Lee, *J. Micromechanics Microengineering*, 2006, **16**, 2403–2410.
23 S. Jambovane, D. J. Kim, E. C. Duin, S. K. Kim and J. W. Hong, *Anal. Chem.*, 2011, **83**, 3358–3364.
24 S. Zeng, B. Li, X. Su, J. Qin and B. Lin, *Lab Chip*, 2009, **9**, 1340.
25 W. S. Lee, S. Jambovane, D. Kim and J. W. Hong, *Microfluid. Nanofluidics*, 2009, **7**, 431–438.
26 X. Sun, K. Tang, R. D. Smith and R. T. Kelly, *Microfluid. Nanofluidics*, 2013, **15**, 117–126.
27 W. C. Cheng, Y. He, A. Y. Chang and L. Que, *Biomicrofluidics*, 2013, **7**, 1–10.
28 M. Sun, S. S. Bithi and S. A. Vanapalli, *Lab Chip*, 2011, **11**, 3949.
29 H. Boukellal, S. Selimović, Y. Jia, G. Cristobal and S. Fraden, *Lab Chip*, 2009, **9**, 331–8.
30 W. Shi, J. Qin, N. Ye and B. Lin, *Lab Chip*, 2008, **8**, 1432.
31 P. Abbyad, R. Dangla, A. Alexandrou and C. N. Baroud, *Lab Chip*, 2011, **11**, 813–821.
32 R. Dangla, S. Lee and C. N. Baroud, *Phys. Rev. Lett.*, 2011, **107**, 1–4.
33 W. Wang, C. Yang and C. M. Li, *Lab Chip*, 2009, **9**, 1504.
34 W.-H. Tan and S. Takeuchi, *Proc. Natl. Acad. Sci.*, 2007, **104**, 1146–1151.
35 T. Franke, , DOI:10.1039/c7lc00378a.
36 K. Liu, H. Ding, Y. Chen and X. Z. Zhao, *Microfluid. Nanofluidics*, 2007, **3**, 239–243.
37 N. Bremond, A. R. Thiam and J. Bibette, *Phys. Rev. Lett.*, 2008, **100**, 1–4.
38 Y.-C. Tan, J. S. Fisher, A. I. Lee, V. Cristini and A. P. Lee, *Lab Chip*, 2004, **4**, 292.
39 Y. C. Tan, Y. L. Ho and A. P. Lee, *Microfluid. Nanofluidics*, 2007, **3**, 495–499.
40 X. Niu, S. Gulati, J. B. Edel and A. J. DeMello, *Lab Chip*, 2008, **8**, 1837.
41 J. Xu, B. Ahn, H. Lee, L. Xu, K. Lee, R. Panchapakesan and K. W. Oh, *Lab Chip*, 2012, **12**, 725–730.
42 F. Guo, K. Liu, X. H. Ji, H. J. Ding, M. Zhang, Q. Zeng, W. Liu, S. S. Guo and X. Z. Zhao, *Appl. Phys. Lett.*, , DOI:10.1063/1.3521283.
43 V. Chokkalingam, B. Weidenhof, M. Krämer, W. F. Maier, S. Herminghaus and R. Seemann, *Lab Chip*, 2010, **10**, 1700.
44 H. Zhou and S. Yao, *Microfluid. Nanofluidics*, 2014, **16**, 667–675.
45 J. Tullis, C. L. Park and P. Abbyad, *Lab Chip*, 2014, **14**, 3285–3289.
46 S. Lee, H. Kim, D. J. Won, J. Lee and J. Kim, *Microfluid. Nanofluidics*, 2016, **20**, 1–9.
47 E. Um, E. Rha, S.-L. Choi, S.-G. Lee and J.-K. Park, *Lab Chip*, 2012, **12**, 1594.
48 P. M. Korczyk, L. Derzsi, S. Jakieła and P. Garstecki, *Lab Chip*, 2013, **13**, 4096.
49 C. Priest, S. Herminghaus and R. Seemann, *Appl. Phys. Lett.*, 2006, **89**, 87–90.
50 M. Chabert, K. D. Dorfman and J. L. Viovy, *Electrophoresis*, 2005, **26**, 3706–3715.
51 W.-H. Tan and S. Takeuchi, *Lab Chip*, 2006, **6**, 757.

52 R. M. Schoeman, E. W. M. Kemna, F. Wolbers and A. van den Berg, *Electrophoresis*, 2014, **35**, 385–392.
53 L. Frenz, A. El Harrak, M. Pauly, S. Bégin-Colin, A. D. Griffiths and J. C. Baret, *Angew. Chemie - Int. Ed.*, 2008, **47**, 6817–6820.
54 P. Singh and N. Aubry, *Electrophoresis*, 2007, **28**, 644–657.
55 J. A. Schwartz, J. V Vykoukal and P. R. C. Gascoyne, 2009, **4**, 11–17.
56 S. K. Cho, H. Moon and C. Kim, 2003, **12**, 70–80.
57 M. L. Cordero, D. R. Burnham, C. N. Baroud and D. McGloin, *Appl. Phys. Lett.*, 2008, **93**, 2006–2009.
58 E. Verneuil, M. L. Cordero, F. Gallaire and C. N. Baroud, *Langmuir*, 2009, **25**, 5127–5134.
59 V. B. Varma, A. Ray, Z. M. Wang, Z. P. Wang and R. V Ramanujan, *Sci. Rep.*, 2016, **6**, 37671.
60 M. Sesen, T. Alan and A. Neild, *Lab Chip*, 2014, **14**, 3325.
61 M. Jang, S. Yang and P. Kim, *Biochip J.*, 2016, **10**, 310–317.
62 E. Tumarkin, L. Tzadu, E. Csaszar, M. Seo, H. Zhang, A. Lee, R. Peerani, K. Purpura, P. W. Zandstra and E. Kumacheva, *Integr. Biol.*, 2011, **3**, 653.
63 S. Atula, R. Grenman and S. Syrjänen, *Exp. Cell Res.*, 1997, **235**, 180–187.
64 K. R. and M. Herlyn, *Cancer Discov.*, 2013, **2**, 775–777.
65 S. Sarkar, P. Sabhachandani, D. Stroopinsky, K. Palmer, N. Cohen, J. Rosenblatt, D. Avigan and T. Konry, *Biomicrofluidics*, 2016, **10**, 1–12.
66 S. Sarkar, V. Motwani, P. Sabhachandani, N. Cohen and and T. Konry, *J Clin Cell Immunol.*, 2015, **6**, 334.
67 B. Dura, S. K. Dougan, M. Barisa, M. M. Hoehl, C. T. Lo, H. L. Ploegh and J. Voldman, *Nat. Commun.*, 2015, **6**, 1–13.
68 H.-H. Jeong, S. H. Jin, B. J. Lee, T. Kim and C.-S. Lee, *Lab Chip*, 2015, **15**, 889–99.
69 J. Q. Boedicker, M. E. Vincent and R. F. Ismagilov, *Angew. Chemie - Int. Ed.*, 2009, **48**, 5908–5911.
70 A. Nanbo, H. Terada, K. Kachi, K. Takada and T. Matsuda, *J. Virol.*, 2012, **86**, 9285–9296.
71 S. Padmanabhan, T. Misteli and D. L. DeVoe, *Lab Chip*, 2017, **17**, 3717–3724.
72 D. E. Cohen, T. Schneider, M. Wang and D. T. Chiu, *Anal. Chem.*, 2010, **82**, 5707–5717.
73 C. Y. Wong and G. Ionut Ciobanu, *Chips Tips Lab Chip*.
74 D. J. Collins, A. Neild, A. deMello, A.-Q. Liu and Y. Ai, *Lab Chip*, 2015, 3439–3459.
75 L. Mazutis, J. Gilbert, W. L. Ung, D. A. Weitz, A. D. Griffiths and J. A. Heyman, *Nat. Protoc.*, 2013, **8**, 870–891.
76 V. Studer, G. Hang, A. Pandolfi, M. Ortiz, W. F. Anderson and S. R. Quake, *J. Appl. Phys.*, 2004, **95**, 393–398.
77 P. Garstecki, M. J. Fuerstman, H. A. Stone and G. M. Whitesides, *Lab Chip*, 2006, **6**, 437–446.
78 S. Timoshenko and S. Woinowsky-Krieger, *Thoery of Plates and Shells*, McGraw-Hill, 1959.